Review of Scientific Instruments ARTICLE scitation.org/journal/rsi

The vacuum arc ion source for indium and tin ions implantation into phase change memory thin films

Cite as: Rev. Sci. Instrum. 90, 123313 (2019); doi: 10.1063/1.5128561
Submitted: 20 September 2019 • Accepted: 2 December 2019 •
Published Online: 26 December 2019

Dmitry Seleznev,[1] Alexander Kozlov,[1] Timur Kulevoy,[1] Alexey Sitnikov,[1,a)] Petr Lazarenko,[2] Yuri Vorobyov,[3] Mikhail Smayev,[4,5] Alexey Yakubov,[2] Alexey Sherchenkov,[2] and Sergey Kozyukhin[6]

AFFILIATIONS

[1]National Research Center "Kurchatov Institute"-ITEP, 117218 Moscow, Russia
[2]National Research University of Electronic Technology, 124498 Zelenograd, Russia
[3]Ryazan State Radio Engineering University, 390005 Ryazan, Russia
[4]Mendeleev University of Chemical Technology of Russia, 125047 Moscow, Russia
[5]Lebedev Physical Institute of RAS, 119991 Moscow, Russia
[6]Kurnakov Institute of General and Inorganic Chemistry of RAS, 119991 Moscow, Russia

Note: Contributed paper, published as part of the Proceedings of the 18th International Conference on Ion Sources, Lanzhou, China, September 2019.
[a)]**Author to whom correspondence should be addressed:** aleksey.sitnikov@itep.ru

ABSTRACT

One of the most prospective electrical and optical nonvolatile memory types is the phase change memory based on chalcogenide materials, particularly $Ge_2Sb_2Te_5$. Introduction of dopants is an effective method for the purposeful change of $Ge_2Sb_2Te_5$ thin film properties. In this work, we used the ion implantation method for the introduction of In and Sn into $Ge_2Sb_2Te_5$ thin films by a Multipurpose Test Bench (MTB) at the National Research Center "Kurchatov Institute"-Institute for Theoretical and Experimental Physics. For Sn and In ion implantation into $Ge_2Sb_2Te_5$, the following MTB elements were used: a vacuum arc ion source, an electrostatic focusing system, and a system for current and beam profile measurements. The MTB parameters for Sn and In ion implantation and its effect on the material properties are presented. Implanted $Ge_2Sb_2Te_5$ thin films were irradiated by femtosecond laser pulses. It was shown that the ion implantation resulted in a decrease in the threshold laser fluence necessary for crystallization compared to the undoped $Ge_2Sb_2Te_5$.

I. INTRODUCTION

One of the most prospective electrical and optical nonvolatile memory types is the phase change memory (PCM) based on the chalcogenide materials, particularly on $Ge_2Sb_2Te_5$ (GST225).[1–3] However, the prospective directions of GST utilization are not limited only to application in memory elements. GST225 thin films are actively used in novel full optical on-chip devices, in particular, microring resonators,[4] Mach-Zehnder interferometers,[5] and surface plasmon waveguide structures;[6] in devices based on the different metastructures operating in the infrared region;[7,8] and for other applications (displays,[9] thermal camouflage,[10] etc.). One of the ways to improve the characteristics of these devices is optimization of the GST225 thin film properties.

Introduction of dopants is an effective method for the purposeful change of the GST225 properties and a possible method for PCM device optimization.[11–16] In particular, the introduction of tin or indium dopants has a significant impact on the electrical and thermal properties of GST225 thin films.[17–19]

Ion implantation is a doping method that is used very often in microelectronics for changing the properties of thin films. By choosing appropriate implantation parameters and film thickness, a uniform Sn or In distribution along the film depth and homogeneous properties can be achieved. Additionally, by varying the dose,

thin-film samples with different impurity concentrations can be obtained.

The preliminary Sn implantation into GST225 was done using a Multipurpose Test Bench (MTB). The results showed that tin ion implantation changes the electrical properties of amorphous GST225 films and their crystallization temperatures. The aim of this work was to investigate the effect of Sn and In ion implantation with different doses on the threshold laser fluence needed for the crystallization of GST225 thin films. This task is important for the optimization of the energy consumption of PCM devices.

II. EXPERIMENTAL

A. Samples preparation

Thin films of the $Ge_2Sb_2Te_5$ composition were prepared by direct current magnetron sputtering at room temperature. The pressure of Ar during the process was 5×10^{-3} Torr, and the sputtering power was 25 W. The amorphous thin films were deposited on the substrates of thermally oxidized silicon (1 μm) with TiN (30 nm)/W (50 nm)/TiN (15 nm) cover. The structure and elemental distribution along the thickness of as-deposited GST225 thin films were checked by X-ray diffraction and Auger electron microscopy, respectively.[20] The thicknesses of thin films were controlled by atomic force microscopy and were about 30 nm. The ion implantation was carried out using the MTB at the National Research Center "Kurchatov Institute"-Institute for Theoretical and Experimental Physics (NRC "Kurchatov Institute"-ITEP).

B. Multipurpose test bench

The structure of the heavy ion source (IS) test-bench is shown in Fig. 1. The MTB is available for time-of-flight (TOF) ion beam spectrum measurements. The MTB includes a vacuum arc ion source, an electrostatic focusing system, a cylindrical deflector, a drift channel, and the system for the current and beam profile measurements.

C. The vacuum arc ion source

The NRC "Kurchatov Institute"-ITEP vacuum arc ion source is used for metal ion beam generation.[21] The vacuum arc IS is shown in Fig. 2. In this ion source, the cathode from the material of interest is fixed in a collet welded to bellows. It enables using the pressure difference between the vacuum and atmosphere area to push the cathode to the surface of the conical aperture in the insulator, separating the cathode and trigger electrodes. Such construction enables

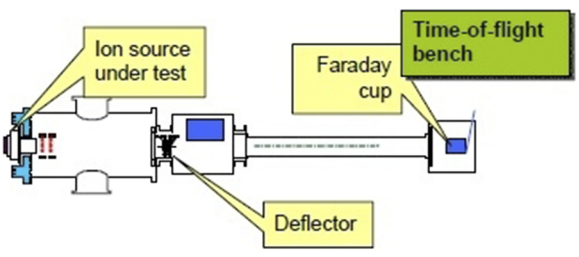

FIG. 1. The structure of the test-bench.

FIG. 2. The NRC "Kurchatov Institute"-ITEP vacuum arc ion source.

using the material of interest as the cathode with any shape, even a piece of foil. The IS can provide metal ion beams with pulse time from 250 μs to 1 ms and a repetition rate up to 25 pps.

The charge state composition of tin and indium beams generated by the vacuum arc ion source was measured by the time-of-flight method using a Heavy Ion Prototype Radio Frequency Quadrupole (HIP-1) linac.[22] The measured charge state distribution for the tin ion beam was 43% of Sn^{1+} and 57% of Sn^{2+}. For the indium ion beam, the distribution was 64.5% of In^{1+}, 34.5% of In^{2+}, and 1% of In^{3+}. The beam profile as well as beam current was also measured. The measured tin ion beam profile is shown in Fig. 3. The target is located between bold vertical lines. The beam uniformity is about 15% in that area. The beam accelerating voltage was calculated by using the SRIM code[23] in order to implant ions on the required depth, taking into account the measured charge state compositions. As a result, ~ 40 kV accelerating voltage was defined for tin ion implantation, while for indium, the value was about 50 kV.

D. Sn and In ion implantation into the GST225 films

To proceed to the implantation process, the profiler was replaced by the combined target, which consists of the target holder, and suppressing and defending rings. The rings were required to suppress the secondary electron emission. The target with the GST225 samples was located at the profiler plane. An −800 V potential was applied to the suppressor ring; the defending ring was at zero potential while the target was used as a beam current collector. The Sn ion implantation was carried out at 41 ± 1 kV accelerating voltage with a beam pulse length of 250 μs and a repetition rate of 2 pps. The pressure in the vacuum tank during the implantation was not worse than 6×10^{-6} mbar.

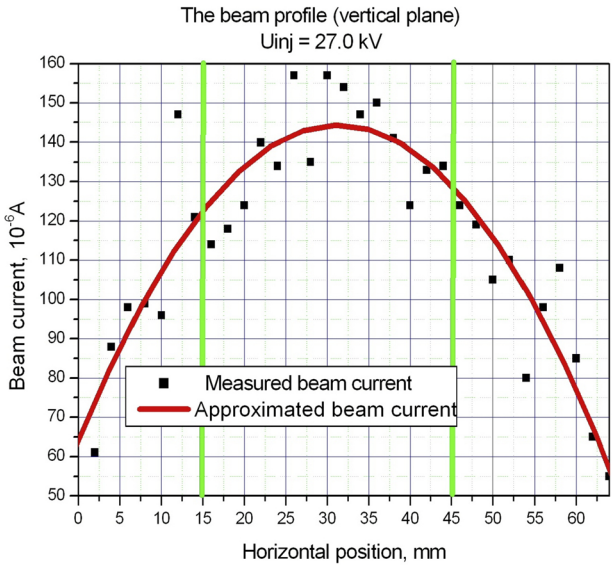

FIG. 3. The Sn ion beam profile.

The typical beam current on the target is shown in Fig. 4. During the first experiment,[20] the total number of implanted beam pulses was equal to 1430, which corresponds to the fluence of 1.4×10^{14} p/cm^2, and provides Sn concentration in the GST225 film of 1 at. %. The preliminary GST225 film investigation had shown that Sn ions were implanted on the required film depth.[20]

Based on the results of the first experiment, the set of tin ion implantation was carried out. The following ion concentrations were achieved: 0.1, 0.5, 1, 2, and 5 at. %. The same set of implantation was carried out for In ions.

E. Methods

The undoped and implanted samples were irradiated by the Yb:KGW femtosecond laser Pharos SP (Light Conversion) with the wavelength of 1030 nm. The pulse duration and the repetition rate were 180 fs and 200 kHz, respectively. Microscopy of the modified areas was performed using an optical microscope with a 110× 0.9 NA objective lens (Carl Zeiss Axiovert 40 MAC). The structural changes were investigated by the Raman study; we used a HORIBA LabRAM HR Evolution spectrometer with 514 nm excitation wavelength and 0.1 mW excitation power.

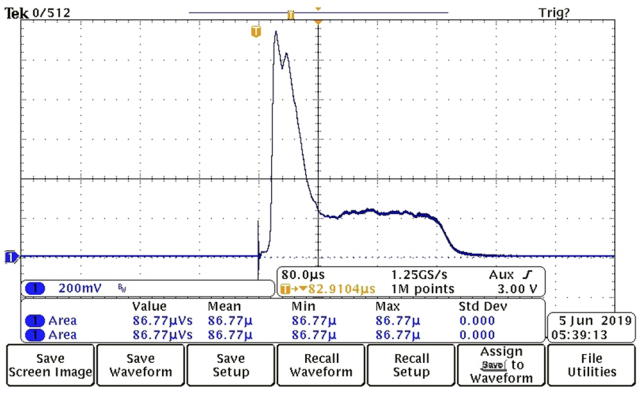

FIG. 4. The In ion beam (250 μs, 5 mA) current on the target.

III. RESULTS AND DISCUSSION

The optical, structural, and morphological changes on the GST225 surface could be distinguished from the several types of marks formed after femtosecond laser irradiation of amorphous thin films. One of the types of marks is the toroidal shell ("ring-shaped roll") with the amorphous central part and crystalline shell. Such shells were obtained for all investigated thin films (Fig. 5). The phase states were determined by the results of Raman spectroscopy.[24]

It is evident from the microphotographs in Fig. 5 that the crystalline area formed as a result of laser treatment is separated from the surrounding amorphous material by a relatively sharp edge. This fact implies that some definite value of the local laser fluence has to be achieved to induce the crystallization of the film material. Below, we refer to this value as the *crystallization threshold*. Optical microscopy showed that the varying number of laser pulses leads to a change in the size of a crystallized area. Therefore, the crystallization threshold is sensitive to the number of pulses. Reduction of the pulse energy leads to a decrease in crystalline spot areas; however, it is not evident whether the crystallization threshold depends on the pulse energy. Hence, we performed measurements of the crystallization threshold value for different pulse energies and pulse numbers for doped and undoped material. Two samples with the same dose of Sn and In were taken for measurements to compare the influence of both dopants on the value of the crystallization threshold.

The calculation of the crystallization threshold was performed as follows: First, for each laser-induced spot on the sample surface, the contour of the crystalline field was determined. Second, the intensity distribution of the utilized laser beam was measured using a USB CCD beam profiler camera, Spiricon SP620U (Ophir), placed in the sample position. Taking into account the laser pulse energy, the local fluence distribution across the sample surface during exposure could be calculated from the obtained intensity profile. This, in turn, allows for the determination of the local fluence value that corresponds to a contour of a crystalline field. This value was taken to be the crystallization threshold.

Figure 6 reports the results of the crystallization threshold calculation. Exponential fits are the guides to the eye. Different symbols correspond to each investigated sample, while different symbols' sizes denote different laser energy values. There are several major conclusions to be drawn from the results shown in Fig. 6.

First of all, the data for different levels of the laser pulse energy overlap, implying that the laser energy does not affect the crystallization threshold value. Indeed, because of the bell-like shape of the laser beam intensity profile, change in the pulse energy modifies only the range of local fluences, specifically, its highest value. Therefore, only the size of crystalline spots is affected by the laser pulse energy, which is demonstrated in Fig. 5. Moreover, the fact that only local fluence matters, regardless of the laser pulse energy, suggests that lateral heat diffusion does not involve in the process of crystalline area formation in our experiments.

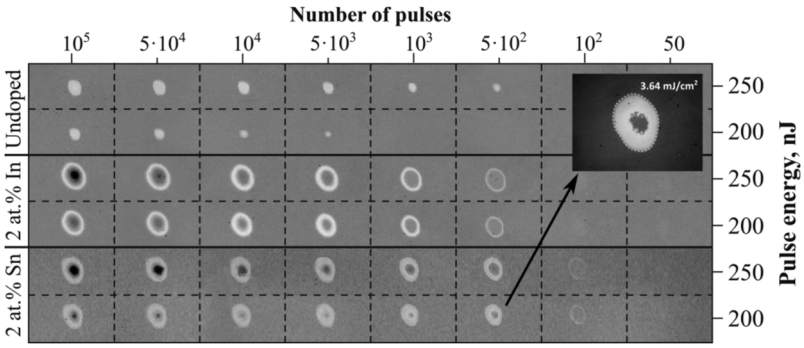

FIG. 5. The optical microscope images of undoped GST225 and GST225 thin films with 2 at. % Sn and In obtained after laser exposure.

Next, the dopant implantation significantly decreases the crystallization threshold over the whole investigated range of pulse numbers. Furthermore, the data provided for both doped samples practically match each other, inferring that the nature of the dopant does not play the fundamental role in the crystallization threshold decrease. We assume, therefore, that the implantation process itself brings down the crystallization threshold, not the change in material composition. Ion beams are known to facilitate crystallization of amorphous films[25] through the introduction of irradiation-induced defects that improve atomic mobility and act as nucleation sites, effectively enhancing phase transition. Parameters of ion bombardment for both Sn and In implantation were very close in our experiments making the corresponding influence similar, thus resulting in the same effect of crystallization threshold lowering regardless of the chemical nature of a dopant.

Another possible explanation for the crystallization threshold lowering of implanted samples is the charged state of introduced dopants. Charged particles are known to decrease the nucleation barrier,[26] thus enhancing the nucleation rate and, accordingly, facilitating crystallization. However, the charge compositions of In and Sn beams cannot be considered equal in our experiment to support this hypothesis.

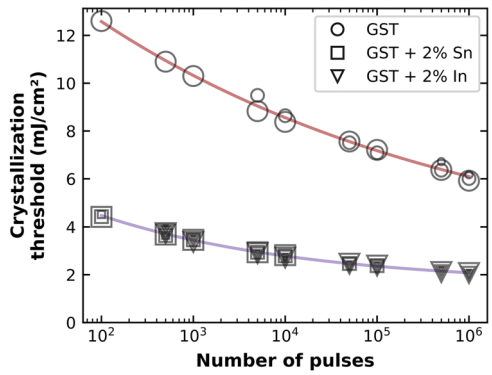

FIG. 6. Crystallization threshold dependence on the number of pulses for samples with different doping. Large symbols (circles, squares, or triangles) correspond to the laser pulse energy Ep = 250 nJ, medium symbols correspond to the energy Ep = 200 nJ, and small symbols correspond to the energy Ep = 150 nJ.

The reason for the crystallization threshold decrease with an increasing number of pulses resides in the mechanism of laser-induced crystallization. After the initial laser pulse, only a stable crystalline nuclei distribution forms, and no discernible features on the initially amorphous film surface are visible. Each subsequent pulse leads to the growth of nuclei, resulting in a staircase-like crystallization process under the train of pulses. More pulses therefore produce more growth steps, making crystallization under lower local fluence possible.

Amorphous marks at the central part of the modified areas do not exhibit clear edges, thus permitting accurate determination of the corresponding local laser fluence. That is why we do not speculate on the threshold for the reamorphization process in this study.

IV. CONCLUSION

The multipurpose test bench with a vacuum arc ion source was used for the introduction of In and Sn ions into GST225 thin films. The implantation regimes providing impurity distributions with different concentrations were determined. The results of the investigation showed that Sn and In ion implantation into GST225 films lead to the decrease of the threshold laser fluence needed for the crystallization by fs-laser pulses. Furthermore, the data provided for both implanted samples practically match each other, inferring that the nature of the dopant does not play a fundamental role in the crystallization threshold decrease.

ACKNOWLEDGMENTS

This study was supported by RFBR (Project No. 18-33-20237\18). The studies of the irradiated samples were performed using equipment of Core Facilities Center “MEMS and electronic components” and “STI Sensory” of MIET and KAMIKS center at NRC KI ITEP.

REFERENCES

[1] P. Guo, A. Sarangan, and I. Agha, Appl. Sci. **9**, 530 (2019).
[2] W. Dong, H. Liu, J. K. Behera, L. Lu, R. J. H. Ng, K. V. Sreekanth, X. Zhou, J. K. W. Yang, and R. E. Simpson, Adv. Funct. Mater. **29**, 1806181 (2019).
[3] M. Wuttig, H. Bhaskaran, and T. Taubner, Nat. Photonics **11**, 465 (2017).
[4] J. Zheng, A. Khanolkar, P. Xu, S. Colburn, S. Deshmukh, J. Myers, J. Frantz, E. Pop, J. Hendrickson, J. Doylend, N. Boechler, and A. Majumdar, Opt. Mater. Express **8**, 1551 (2018).

[5]H. Zhang, L. Zhou, B. M. A. Rahman, X. Wu, L. Lu, Y. Xu, J. Xu, J. Song, Z. Hu, L. Xu, and J. Chen, IEEE Photonics J. **10**, 1 (2018).
[6]M. Rudé, R. E. Simpson, R. Quidant, V. Pruneri, and J. Renger, ACS Photonics **2**, 669 (2015).
[7]A. V. Pogrebnyakov, J. A. Bossard, J. P. Turpin, J. D. Musgraves, H. J. Shin, C. Rivero-Baleine, N. Podraza, K. A. Richardson, D. H. Werner, and T. S. Mayer, Opt. Mater. Express **8**, 2264 (2018).
[8]Z. Guo, X. Yang, F. Shen, Q. Zhou, J. Gao, and K. Guo, Sci. Rep. **8**, 12433 (2018).
[9]P. Hosseini, C. D. Wright, and H. Bhaskaran, Nature **511**, 206 (2014).
[10]Y. Qu, Q. Li, L. Cai, M. Pan, P. Ghosh, K. Du, and M. Qiu, Light: Sci. Appl. **7**, 26 (2018).
[11]R. Sinha-Roy, A. Louiset, M. Benoit, and L. Calmels, Phys. Rev. B **99**, 245124 (2019).
[12]S. Kumar, P. Sharma, and V. Sharma, Results Phys. **13**, 102276 (2019).
[13]K. Ding, K. Ren, F. Rao, Z. Song, L. Wu, B. Liu, and S. Feng, Mater. Lett. **125**, 143 (2014).
[14]P. Guo, J. A. Burrow, G. A. Sevison, A. Sood, M. Asheghi, J. R. Hendrickson, K. E. Goodson, I. Agha, and A. Sarangan, Appl. Phys. Lett. **113**, 171903 (2018).
[15]A. Babich, A. Sherchenkov, S. Kozyukhin, P. Lazarenko, O. Boytsova, and A. Shuliatyev, J. Therm. Anal. Calorim. **127**, 283 (2017).
[16]M. Agati, F. Renaud, D. Benoit, and A. Claverie, MRS Commun. **8**, 1145 (2018).
[17]Q. Yin and L. Chen, J. Mater. Sci.: Mater. Electron. **29**, 16523 (2018).
[18]N. Bai, F. R. Liu, X. X. Han, Z. Zhu, F. Liu, X. Lin, and N. X. Sun, Appl. Surf. Sci. **316**, 202 (2014).
[19]P. I. Lazarenko, A. A. Sherchenkov, S. A. Kozyukhin, A. V. Babich, H. P. Nguen, S. P. Timoshenkov, D. G. Gromov, A. O. Yakubov, and D. Y. Terekhov, J. Phys.: Conf. Ser. **690**, 012006 (2016).
[20]A. Sitnikov, D. Dronova, P. Fedin, A. Kozlov, S. Kozyukhin, T. Kulevoy, P. Lazarenko, D. Selesnev, A. Sherchenkov, and A. Yakubov, in *26th Russian Particle Accelerator Conference RUPAC2018, Protvino, Russia* (JACoW, 2018), pp. 230–232.
[21]V. A. Batalin, J. N. Volkov, T. V. Kulevoy, and S. V. Petrenko, Rev. Sci. Instrum. **65**, 3104 (1994).
[22]R. P. Kuibeda, S. L. Andrianov, P. A. Fedin, B. K. Kondratiev, A. V. Kozlov, A. A. Nikitin, B. B. Chalih, A. L. Sitnikov, S. V. Rogozhkin, and T. V. Kulevoy, in *Proceedings of RuPAC2014, Obninsk, Kaluga Region, Russia* (JACoW, 2014), pp. 97–99.
[23]See http://www.srim.org for information about the interactions of ions with matter.
[24]S. Kozyukhin, P. Lazarenko, Y. Vorobyov, A. Baranchikov, V. Glukhenkaya, M. Smayev, A. Sherchenkov, Y. Sybina, A. Polohin, and V. Sigaev, Opt. Laser Technol. **113**, 87 (2019).
[25]R. G. Elliman, S. T. Johnson, A. P. Pogany, and J. S. Williams, Nucl. Instrum. Methods Phys. Res., Sect. B **7-8**, 310 (1985).
[26]D. Kashchiev, *Basic Theory with Applications* (Butterworth-Heinemann, Oxford, 2000).